Molecular dynamics of a model dimerizing fluid

C. E. Bertrand and Y. Liu

Citation: The Journal of Chemical Physics **142**, 044503 (2015); doi: 10.1063/1.4906608
View online: http://dx.doi.org/10.1063/1.4906608
View Table of Contents: http://scitation.aip.org/content/aip/journal/jcp/142/4?ver=pdfcov
Published by the AIP Publishing

Molecular dynamics of a model dimerizing fluid

C. E. Bertrand[1] and Y. Liu[1,2,a)]
[1]*NIST Center for Neutron Research, National Institute of Standards and Technology, Gaithersburg, Maryland 20899, USA*
[2]*Department of Chemical and Biomolecular Engineering, University of Delaware, Newark, Delaware 19716, USA*

(Received 29 October 2014; accepted 13 January 2015; published online 27 January 2015)

A model dimer forming fluid has been investigated by continuous molecular dynamics simulations. This study emphasizes the volume fraction and temperature dependence of the dynamic properties of the system, including the self and collective diffusion coefficients and the forward and reverse rate constants. The self and collective diffusion coefficients are found to be well described by a monomer fraction controlled interpolation formula. The forward rate constant (dimer formation) is found to be weakly temperature dependent and strongly volume fraction dependent. The opposite holds for the reverse rate constant. The dimer and monomer decay rates are not found to affect the intermediate scattering functions at the conditions studied. [http://dx.doi.org/10.1063/1.4906608]

I. INTRODUCTION

The presence of short-ranged highly directional attractive interactions can have a profound effect on the phase behavior of fluids.[1] In some cases, these interactions lead to the formation of equilibrium clusters. Such cluster formation has been observed in a wide variety of fluids including hydrogen-bonding molecular liquids, like water[2] and hydrofluoric acid,[3] colloidal suspensions of monoclonal antibodies,[4] and synthetic patchy particles, e.g., Janus particles.[5] Notably, cluster formation can also be found in systems with isotropic interactions, when the interaction potential is characterized by short-range attraction and long-range repulsion.[6,7]

A cluster can be defined as a contiguous set of associating particles (molecules). The strength of association is typically intermediate to van der Waals interactions and covalent bonds. Hence, the degree of association is generally sensitive to temperature and particle density. While a preferred cluster size may exist, a broad cluster size distribution is found in many systems. In contrast to the irreversible processes associated with the formation of flocs or aggregates in colloids, the formation of so-called equilibrium clusters is reversible.

Our understanding of associating fluids has been substantially furthered through the study of primitive and coarse-grained models. A general theoretical treatment of associating fluids was developed by Wertheim[11–14] based on the addition short-range association sites to a model reference liquid, e.g., hard-sphere or Lennard-Jones. This approach to modeling the features of associating fluids underpins the statistical associating fluid theory (SAFT), which has been successful at describing the phase behavior of associating molecular fluids.[15,16] In recent years, a new focus on patchy colloids[1] has emerged and new models, such as the Kern-Frenkel model,[17] that ease restrictions on bond saturation and valency have been investigated. Computer simulations have been a primary tool for analyzing the properties of these models.

Much attention has been devoted to the phase behavior of cluster forming systems. Less has focused on the dynamics of clusters. One of the challenges surrounding the characterization of cluster dynamics is the distribution of cluster sizes and the resulting ambiguity in defining cluster dynamic properties for a system with isotropic interactions. Additional complexities arise from the availability of multiple decay and growth modes for a cluster of a given size and geometry. For instance, a cluster may decay through either the departure of a single particle on the surface or through the fragmentation of the cluster into two smaller clusters of roughly equal sizes. Recent experiments on concentrated lysozyme solutions have led to a proposed classification of clusters as either transient, dynamic, or permanent.[18] Without an appropriate model of cluster dynamics, the general applicability of such a scheme remains uncertain. An important first step towards understanding dynamics in complex cluster forming systems is the characterization of dynamics in the well-defined dimerizing system.

The most basic cluster is a dimer. Reversible dimerization is found in both molecular and colloidal fluids. For example, the reaction $2NO_2 \rightleftharpoons N_2O_4$ was first studied over a century ago.[8] More recently, patchy particles capable of exclusively forming dimers have been synthesized.[9] The effects of dimer formation in colloidal suspensions can significantly impact potential applications. On the basis of neutron spin echo spectroscopy measurements, Yearly *et al.* have reported dimer formation in concentrated solutions of monoclonal antibodies.[10] In this system, the cluster formation leads to a substantial increase in viscosity. This in turn limits the biopharmaceutical applications of the protein solution. From a theoretical perspective, the dimer system has the advantage that the cluster size is unique (a cluster of degree two) and that the lifetime of a cluster can be rigorously defined.

Surprisingly, the dynamics of model dimerizing systems have received relatively little attention. Liu *et al.*[19] developed

a)Author to whom correspondence should be addressed. Electronic addresses: yunliu@udel.edu and yunliu@nist.gov

an event-driven molecular dynamics algorithm and applied it to the Wertheim dimer model as a test case, before moving on to more complex systems.[20] Subsequently, Li and Nies[21,22] made extensive continuous molecular dynamics simulations of a dimerizing model inspired by the discontinuous models employed in SAFT-based theories. This work employed a Lennard-Jones reference potential and extensively studied the effect of varying the depth of the association potential relative to the Lennard-Jones energy scale. Not surprisingly, the static properties of model dimerizing systems are very well studied. In fact, early on, Wertheim applied his theory to a fluid of dimerizing hard-spheres with a single square-well association site.[23]

In this work, we present continuous molecular dynamics simulations of a model dimerizing fluid. We address the dependence of structural and dynamic properties on temperature and volume fraction. Furthermore, we investigate the connection between structure, particle diffusion, and the kinetics of bond formation and dissociation. In addition to examining some detailed information that is, at least currently, only available to computer simulations, we also focus on the behavior of experimentally accessible correlation functions, with an eye towards identifying experimentally relevant signatures of cluster formation.

II. THE MODEL

To describe a system of dimerizing particles, we use a model previously employed by Russo *et al.*,[24] which these authors used to study reversible colloidal gels. Each particle consists of two interaction sites separated by a fixed distance δ. We refer to these as *core* and *association* sites. The core-core interactions are described by a soft-core potential with energy-scale ϵ and length-scale σ,

$$V_{cc} = \epsilon\left(\frac{\sigma}{r_{cc}}\right)^n, \tag{1}$$

where r_{cc} is the distance between core sites, and the association-association interactions are described by an attractive potential well

$$V_{aa} = -A\exp\left[-\left(\frac{r_{aa}}{d}\right)^p\right], \tag{2}$$

where r_{aa} is the distance between association sites. The core and association sites do not interact with each other, i.e., $V_{ac} = V_{ca} = 0$. A schematic of the associating particle is shown in Figure 1. For $n \gg 1$ and $p \gg 1$, $V_{cc}(r)$ approaches the potential for two hard spheres of diameter σ and $V_{aa}(r)$ limits to a square-well of depth A and range d. Hence, this model is a softened version of the model originally investigated by Wertheim.[23] Some of the structural features of this model are discussed in the supplementary material.[25]

The mass of the core and association sites can be set independently. The particle mass and moment of inertia do not enter into Monte Carlo calculations. They are, however, essential for propagating molecular dynamics trajectories. In general, the particle center of mass is located between the two sites, as set by the relative masses of the sites. This can lead to small scale librational motions. In our simulations, the

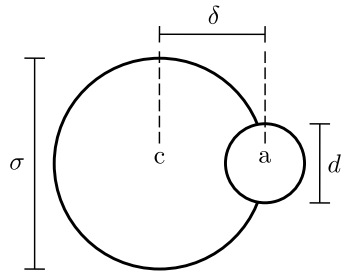

FIG. 1. Schematic of the model dimerizing particle. The relative sizes, d and σ, of the association site, a, and core site, c, are not drawn to scale.

core and association sites have equal masses and the total mass of a particle is denoted by m. This choice matches that adopted by Li and Nies.[22] In an earlier work,[21] these authors studied the effect of varying the mass ratio and found that the mass ratio does effect the quantitative, but not qualitative, behavior of properties like the long time diffusion coefficient. In theory, the association site could be forced to rotate around the core site by adding a collinear, non-interacting, massive "dummy" site. However, this comes at an additional, and apparently unnecessary, computational expense.

In this work, distances are measured in units of σ, mass in units of m, energy in units of ϵ. Additionally, time is measured in units of $\tau = \sigma\sqrt{m/\epsilon}$. Using the soft-core energy scale ϵ, we define a dimensionless temperature by $T^* = k_B T/\epsilon$, where k_B is Boltzmann's constant. Our choice of units leaves δ, A, d, n, and p in Eqs. (1) and (2) as free parameters. The values of these parameters used in this work are $\delta = 0.5\sigma$, $A = 10\epsilon$, $d = 0.1\sigma$, $n = 50$, and $p = 2$. This choice of parameters ensures that the association site is short-ranged. The total potential energy of two molecules with collinear interaction sites is shown in Figure 2. Only a small fraction of the effective surface area of the core site is covered by the association site (~3%). This ensures that only two association sites can interact simultaneously. Therefore, the only clusters formed are dimers.

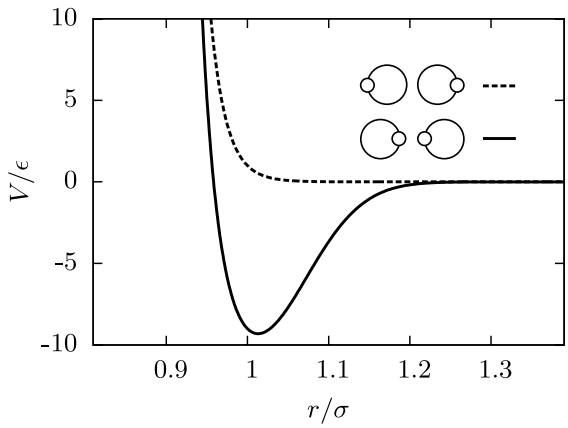

FIG. 2. Total potential energy for two particles with collinear sites as a function of core-core separation r. The dashed curve corresponds to association sites on opposite sides of the core sites. The full curve corresponds to association sites on the same side of the core sites.

A. Reference systems

In addition to the associating model defined by Eqs. (1) and (2), we have studied two related reference systems: *non-associating* and *permanent dimer*. The non-associating model sets $V_{aa}(r) = 0$, but leaves the massive association site attached to the core. The structural and thermodynamic properties of this model are identical to those of a single site soft-core model described by Eq. (1). However, the dynamics are affected by the massive dummy association site. At high temperatures, the behavior of our model approaches that of the non-associating model. The permanent dimer models two permanently associated particles. This is accomplished with a collinear four site "molecule." Two of the sites are massive and non-interacting. These reproduce the total mass and moment of inertia of a dimer with a core-core separation corresponding to the minimum in the molecular interaction energy, specifically, $r_{min} = 1.013\sigma$. The remaining two sites are virtual sites that interact through the soft-core potential, Eq. (1). This permanent dimer model may appear unnecessarily cumbersome, since the same mass, moment of inertia, and interactions could be achieved with three sites. However, the LINCS constraint algorithm used in our simulations is singular for linear molecules. The use of virtual sites provides an effective work around.

III. SIMULATION DETAILS

Molecular dynamics simulations were performed with Gromacs 4.6.3.[26] Details regarding the implementation of our model can be found in the supplementary material.[25] All simulations were performed in the NVT ensemble. Each periodic simulation box contained $N = 2048$ dimerizing particles. The behavior of the system was studied at different values of the temperature and volume fraction $\phi = (\pi/6)\rho\sigma^3$, where $\rho = N/V$ is the number density of particles. Specifically, four volume fractions, $\phi = 0.1$, 0.2, 0.3, and 0.4, and seven temperatures $T^* = 1.5$, 1.0, 0.9, 0.8, 0.7, 0.6, and 0.5 were used. For each volume fraction, the system was initialized by placing the molecules on a face-centered cubic lattice and assigning velocities from a Boltzmann distribution at T^*. Measurements were made over the course of 2.5×10^6 MD steps following an equilibration period. The final frame of each trajectory served as the initial frame for the next lowest temperature. Equilibration of the system was monitored with the total potential energy. The longest required equilibration time was 2.5×10^7 MD steps at $\phi = 0.1$ and $T^* = 0.5$. The production runs were thermostated with the Nose-Hoover thermostat ($\tau_T = 250$ MD steps). Intraparticle constraints were imposed using LINCS.

IV. MONOMER FRACTION

The extent of dimerization in the system is characterized by the monomer fraction $X = N_M/N$, where N_M is the number of monomers. For our model, the definition of a dimer is slightly subjective, as compared to models with square-well association sites. We take $r_b \simeq 0.2\sigma$ as the bonding distance. When the separation between two association sites is less than r_b, we say that the particles are bonded. This distance corresponds to a reduction of the interaction strength by roughly 95% relative to the value at the bottom of the potential well (cf. Fig. 2). Further justification for our choice of r_b can be found in the supplementary material.[25] Calculated monomer fractions are shown in Figure 3. The degree of bonding increases with decreasing temperature and increasing volume fraction.

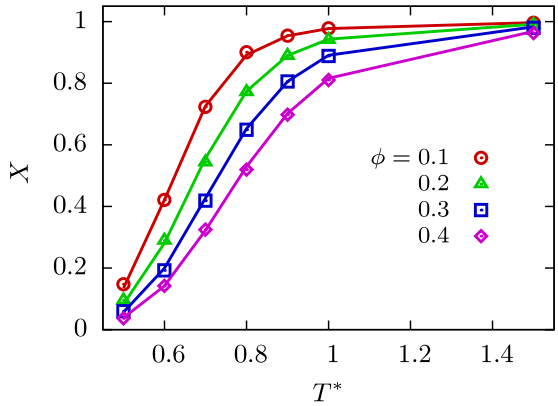

FIG. 3. Monomer fraction of the associating model as a function of reduced temperature. The points are calculated from our simulations. The line segments connect predictions from the Wertheim theory, Eq. (3).

In Wertheim's theory of dimerization, the monomer fraction is given by

$$X = \frac{-1 + \sqrt{1 + 4\rho\Delta}}{2\rho\Delta}, \tag{3}$$

where

$$\Delta = 4\pi \int dr\, r^2 g_0(r) \langle f(r) \rangle_{\Omega_1,\Omega_2}, \tag{4}$$

and ρ is the number density. In Eq. (4), $g_0(r)$ is the radial distribution function of the reference system ($V_{aa} = 0$), $\langle \cdots \rangle_{\Omega_1,\Omega_2}$ is an unweighted angular average, and $f(r)$ is the Mayer function

$$f(r) = \exp(-\beta V_{aa}(r)) - 1. \tag{5}$$

Once X is known as a function of ϕ and T, various thermodynamic properties can be calculated. We have calculated X numerically with $g_0(r)$ taken from our simulations of the non-associating reference system. The results are shown in Figure 3. The agreement between the theory and our simulations is very good.

For our forthcoming discussion of dynamic phenomena, it is instructive to consider fluctuations in the monomer fraction, since these fluctuations determine the amplitude of the relevant dynamic correlation function. The calculated standard deviation of the monomer fraction is shown in Figure 4. By definition, $\sqrt{\langle (\Delta X)^2 \rangle} = \sqrt{\langle (\Delta N_M)^2 \rangle}/N$. Therefore, the total number of bonded particles fluctuates by at most ~1% of the total number of particles. We note that the fluctuations generally increase with volume fraction and that they exhibit a maximum in the temperature range where the monomer fraction changes most rapidly. However, the calculation of these fluctuations suffers from poor statistics,

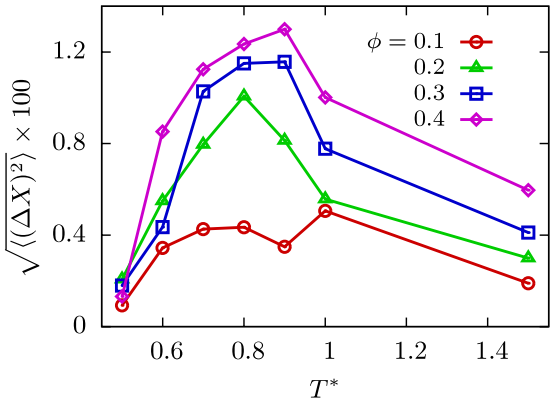

FIG. 4. Standard deviation of the monomer fraction as a function of reduced temperature. The points are calculated from our simulations. The connecting lines are a guide to the eye. In general, the magnitude of the fluctuations is relatively small.

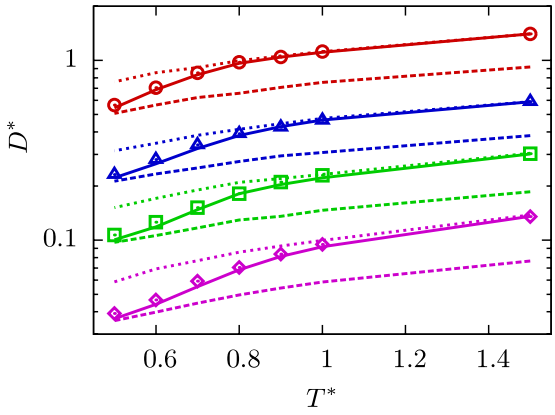

FIG. 5. The reduced self-diffusion coefficient $D^* = D_s\tau/\sigma^2$ as a function of reduced temperature. The points are calculated from our simulations of the associating system. The solid lines correspond to the predictions of Eq. (9). For comparison, results from the non-associating (monomer) and permanent dimer (dimer) models are shown as dotted and dashed lines, respectively. The meaning of the symbols is the same as in Fig. 4.

and we cannot say with certainty whether the non-monotonic behavior in ϕ seen at low T is physically meaningful.

V. DYNAMICS

A. Single particle dynamics

The self-intermediate scattering function (SISF) characterizes length-scale dependent single particle dynamics and is defined by

$$F_s(Q,t) = \frac{1}{N}\left\langle \sum_j^N \exp\left(i\mathbf{Q}\cdot[\mathbf{R}_j(t) - \mathbf{R}_j(0)]\right)\right\rangle, \tag{6}$$

where $\mathbf{R}_i$ is position of the ith core-site and the magnitude of the scattering vector Q determines the (inverse) length scale probed. In the case of Fickian diffusion, the Q dependence of the SISF is accounted for by the Gaussian approximation[27]

$$F_s(Q,t) \simeq \exp\left(-\frac{1}{6}\left\langle[\mathbf{R}(t) - \mathbf{R}(0)]^2\right\rangle Q^2\right). \tag{7}$$

For all Q studied, our system follows the Gaussian approximation closely. Consequently, we have concentrated on the particle mean-squared displacement without a loss of generality. In the long time limit, the mean-squared displacement is related to the self diffusion coefficient D_s by

$$\lim_{t\to\infty}\left\langle[\mathbf{R}(t) - \mathbf{R}(0)]^2\right\rangle = 6D_s t. \tag{8}$$

We have measured the self-diffusion coefficients in our simulations by making linear fits of the long time (>80τ) mean-squared displacement. The results are shown in Fig. 5. Additionally, we have measured D_s for the two reference systems described in Sec. II A, namely, the non-associating and permanent dimer systems. The self diffusion coefficient of the associating system interpolates smoothly between the bounds established by the non-associating (M) and permanent dimer (D) systems. The associating self-diffusion coefficient can be estimated by using the monomer fraction to interpolate between these two limiting cases,

$$D_s = X D_M + (1 - X) D_D. \tag{9}$$

This relationship describes the observed values of D_s quite well. It is also what would be expected from non-interacting mixtures of permanent dimers and monomers with the correct monomer fraction. This seems to indicate that the dynamic nature of the bonds in our system does not significantly affect the self diffusion coefficient. The ratio between non-associating and permanent dimer diffusion coefficients varies between $D_M/D_D = 1.5$ for $\phi = 0.1$, $T = 1.5$ and $D_M/D_D = 1.8$ for $\phi = 0.4$, $T = 1.5$. Equation (9) appears to systematically underestimate our measured values by roughly 5% at lower temperatures. This may stem from the fact that a bond between two dimerized particles is somewhat flexible, whereas the bonds in permanent dimers are rigid. Intuitively, one expects flexible dimers to diffuse more easily than rigid dimers in dense environments. In this context, permanent dimers bound by a harmonic potential might prove to be a better reference system than our rigidly bound dimers.

B. Collective dynamics

The many-body analog of the SISF is the full intermediate scattering function (FISF)

$$F(Q,t) = \frac{1}{N}\left\langle \sum_{i,j}^N \exp\left(i\mathbf{Q}\cdot[\mathbf{R}_j(t) - \mathbf{R}_i(0)]\right)\right\rangle. \tag{10}$$

The FISF is related to the van Hove function $G(\mathbf{r},t)$ by a spatial Fourier transform,[34]

$$F(Q,t) = \int d\mathbf{r}\, G(\mathbf{r},t)\exp(-i\mathbf{Q}\cdot\mathbf{r}). \tag{11}$$

We have calculated the FISF is our system via Eq. (11). The resulting correlation functions are all well described by a single exponential decay in the approximation $F(Q,t) \simeq S(Q)\exp[-\Gamma(Q)t]$. Examples of the extracted decay rates Γ are shown in Figure 6. The extracted decay rates exhibit a dip in the Q range corresponding to the main structure factor peak (cf. supplementary material[25]), a phenomenon known as de Gennes narrowing.[28] As in the case of the self

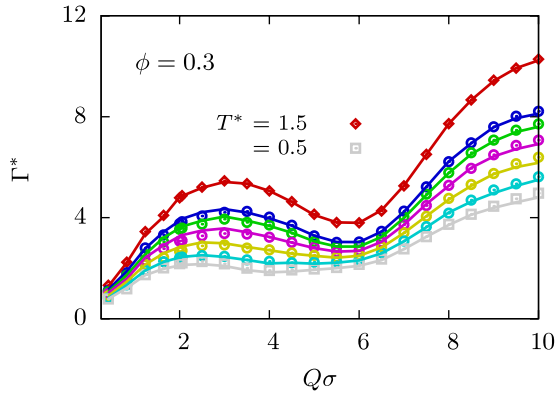

FIG. 6. The reduced collective decay rate $\Gamma^* = \Gamma\tau$ as a function of wavenumber. Points are calculated from our simulations. The unlabeled points between $T^* = 1.5$ and 0.5 are from intermediate temperatures. The solid curves correspond to the predictions of Eq. (12).

diffusion coefficient, the collective decay rates follow a linear interpolation between the non-associating (M) and permanent dimer (D) cases, specifically,

$$\Gamma(Q) \simeq X\Gamma_{\mathrm{M}}(Q) + (1-X)\Gamma_{\mathrm{D}}(Q). \tag{12}$$

Curves corresponding to Eq. (12) are also shown in Fig. 6. We conclude that the dynamic nature of the dimerization process does not manifest itself in the FISF either, at least over the studied Q range. In other words, the rates of dimer formation and dissociation cannot be found by analyzing the diffusive behavior of the system. We note that the interpolation formulas Eqs. (9) and (12) can be used to extract the monomer fraction X, if the diffusion coefficients or collective decay rates are known for the monomer and dimer species independently.

VI. ASSOCIATION KINETICS

A. Mass balance

Reversible dimerization can be described in terms of a "chemical" reaction between the monomer species M and the dimer species D,

$$2\mathrm{M} \underset{k_-}{\overset{k_+}{\rightleftharpoons}} \mathrm{D}, \tag{13}$$

where k_+ and k_- are the forward and reverse rate constants, respectively. We denote the concentrations of monomers and dimers by $[\mathrm{M}] = N_{\mathrm{M}}/V$ and $[\mathrm{D}] = N_{\mathrm{D}}/V$. The law of mass action relates the ratio of rate constants to *equilibrium* concentrations by

$$\frac{k_+}{k_-} = \frac{\rho[\mathrm{D}]}{[\mathrm{M}]^2} = \frac{1-X}{2X^2} = \frac{\rho\Delta}{2}. \tag{14}$$

The last equalities follow from the identities $[M] = \rho X$ and $[D] = \frac{1}{2}\rho(1-X)$ and Eq. (3). Note that we have introduced an additional factor of ρ, as compared to the canonical definition of the rate constants, so that k_+ and k_- have the same units. When $\rho\Delta = 2$, the rate constants are equal $k_+ = k_-$ and the system is half-dimerized, i.e., $X = 0.5$. Equation (14) makes it apparent that the quantity $\rho\Delta/2$ is simply the equilibrium constant for the system (cf. a statistical mechanical treatment of chemical equilibrium[29]).

B. Rate constants

In theory, the rate constants in our system can be found by studying equilibrium fluctuations in the monomer fraction.[30] However, the small magnitude of the monomer fraction fluctuations (cf. Figure 4) renders this approach overly challenging. Instead, we will first determine the rate constants from non-equilibrium temperature quench measurements.

The relaxation of the monomer concentration is described by the mass balance equation[30]

$$\frac{\partial[\mathrm{M}]}{\partial t} = -2\rho^{-1}k_+[\mathrm{M}]^2 + 2k_-[\mathrm{D}]. \tag{15}$$

Note that Eq. (14) satisfies the equilibrium condition $\partial[\mathrm{M}]/\partial t = 0$. We can rewrite the above equation in terms of the monomer fraction as

$$\frac{\partial X}{\partial t} = -2k_+X^2 + k_-(1-X). \tag{16}$$

Following a temperature quench from T_{i} to T_{f} at $t = 0$, the relaxation of the monomer fraction from X_{i} to X_{f} is found by integrating Eq. (16) to be

$$X(t) = X_{\mathrm{f}} + \frac{(X_{\mathrm{i}} - X_{\mathrm{f}})e^{-\omega t}}{1 + B(1-e^{-\omega t})}, \tag{17}$$

where

$$\omega = 4k_+X_{\mathrm{f}} + k_- \tag{18}$$

and

$$B = \frac{2k_+(X_{\mathrm{i}} - X_{\mathrm{f}})}{4k_+X_{\mathrm{f}} + k_-}. \tag{19}$$

The rate constants in the definitions of ω and B are evaluated at T_{f}.

We have measured the monomer fraction relaxation following a quench between successive temperature points. Examples of the resulting $X(t)$ curves are shown in Figure 7. The initial system configurations were taken from the production trajectories at the initial (higher) temperature. The initial velocities of the particles were then randomly selected from a Boltzmann distribution at the final (lower) temperature and the system was propagated forward at this temperature. Each curve represents the average of 10 measurements with initial configurations separated by 1.25×10^5 MD steps.

A significant difference between X_{i} and X_{f} is required to extract meaningful values of ω. Hence, we have restricted ourselves to $T_{\mathrm{f}} = 0.8$, 0.7, 0.6, and 0.5 (cf. Fig. 3). The factor B characterizes the non-linear response of the system. By combining Eqs. (19) and (14), we find

$$B = \frac{(1-X_{\mathrm{f}})}{X_{\mathrm{f}}(2-X_{\mathrm{f}})}(X_{\mathrm{i}} - X_{\mathrm{f}}). \tag{20}$$

Therefore, non-linear relaxation effects are negligible for $(X_{\mathrm{i}} - X_{\mathrm{f}}) \ll 1$, except when X_{f} approaches 0. We have fit the measured $X(t)$ curves at these temperatures with Eq. (17), treating X_{f}, X_{i}, and ω as free parameters and using the constraint Eq. (20). Examples of the resulting fit curves are

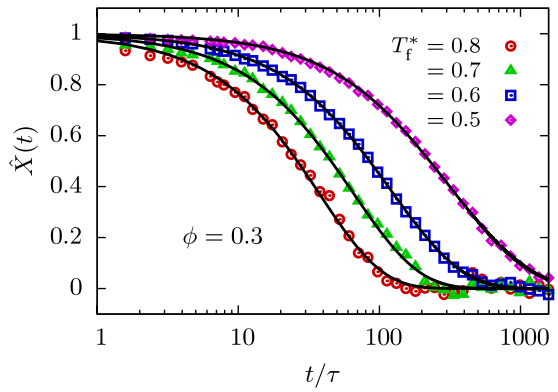

FIG. 7. Relaxation of the normalized monomer fraction $\hat{X}(t) = (X(t) - X_f)/(X_i - X_f)$. The points are calculated from our simulations. The lines are fits to Eq. (17). These fits are used to extract the rate constants shown in Fig. 8.

shown in Figure 7. The fit quality at the lowest temperatures is significantly reduced if the nonlinear contribution is neglected, i.e., if $B = 0$. The extracted values of X_f and X_i agree well with the X values in Fig. 3.

Relationships between ω and the rate constants k_+ and k_- are found by combining Eqs. (18) and (14) to yield

$$k_+ = \left(\frac{1 - X_f}{4X_f - 2X_f^2}\right)\omega \tag{21}$$

and

$$k_- = \left(\frac{X_f}{2 - X_f}\right)\omega. \tag{22}$$

We have calculated k_+ and k_- using the values of ω and X_f extracted from our fits. The results are shown in Fig. 8. We note that Eq. (20) forces the fitted ratio k_+/k_- to agree with the Wertheim prediction, Eq. (14). The forward rate constant k_+ (dimer formation) is strongly volume fraction dependent and weakly temperature dependent. In contrast, the reverse rate constant k_- (dissociation) is weakly dependent on the volume fraction, but strongly dependent on temperature. The differences in the behavior of the two rate constants can be interpreted in terms of the different associated decay mechanisms. The formation of bonds is primarily limited by

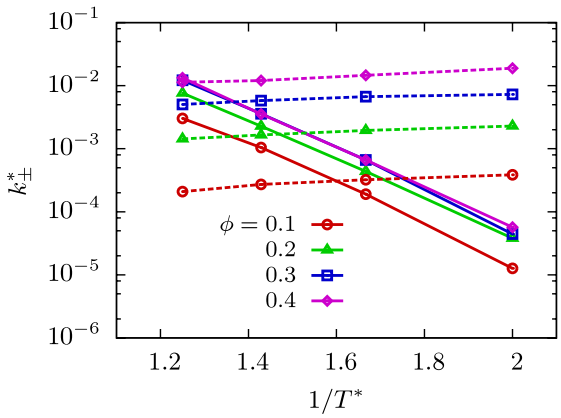

FIG. 8. Arrhenius plot of the reduced rate constants $k^* = k\tau$. The connecting lines are guides to the eye. Solid lines represent the reverse rate constant k_- and dashed lines represent the forward rate constant k_+.

the diffusive processes in the system and the rate at which association sites are able to find each other. Bond breaking on the other hand is an activated process that depends on an energy barrier being overcome during a number of escape attempts.

Our approach to measuring the rate constants in this section is similar to that employed by Sciortino *et al.*[31] in their investigations of mixtures of two and three site associating particles. To model the time evolution of clusters formed in their system, they utilized a theory of polymer aggregation kinetics due to van Dongen and Ernst.[32] In the dimer limit, the basic equations of this theory reduce to those found in this section. Interestingly, Sciortino *et al.* did not observe any volume fraction dependence for k_- in contrast to Fig. 8. This difference may be due to their use of Brownian dynamics as compared to our use of Hamiltonian dynamics. Under Hamiltonian dynamics, dimers dissociate through collisions with other particles. The frequency of these collisions increases with increasing density. In contrast, under Brownian dynamics, dimers can also dissociate as a result of the random forces acting on the particles. These forces are intended to simulate the effect of a solvent acting on a colloidal particle. If the Brownian forces induce dissociation more rapidly than collisions do, the dissociation rate will not depend strongly on density.

C. Dimer and monomer lifetimes

The average lifetimes of the dimer and monomer states are closely related to the rate constants. In this subsection, we explore this connection. First, we define two phase space operators, which are functions of the association-site coordinates $\mathbf{R}(t)$. The dimer operator is given by

$$d_i(t) = \sum_j^N \Theta\left(r_b - \left|\mathbf{R}_j(t) - \mathbf{R}_i(t)\right|\right), \tag{23}$$

where the Heavyside function Θ has a value of 1 for positive arguments and 0 for negative arguments. Thus, $d_i(t)$ is 1 if the ith particle is dimerized at time t and 0 otherwise. In terms of the dimer operator, the monomer operator is

$$m_i(t) = 1 - d_i(t). \tag{24}$$

It is also useful to introduce the first passage time τ_i^a of the ith particle out of the monomer or dimer state. The dimer and monomer correlation functions are defined as

$$C_a(t) = \sum_i^N a_i(t)a_i(0)\Theta\left(t - \tau_i^a\right), \tag{25}$$

where $a_i(t)$ denotes either the dimer operator $d_i(t)$ or the monomer operator $m_i(t)$. The inclusion of $\Theta\left(t - \tau_i^a\right)$ ensures that when $a_i(t)$ changes from 1 to 0, it is not double counted when it eventually changes back. This distinction is important because theories of kinetic phenomena can often be formulated in terms of a first passage problem. The characteristic decay rates, Γ_a, of these correlation functions are defined by the relaxation equation

$$\frac{\partial C_a(t)}{\partial t} = -\Gamma_a C_a(t). \tag{26}$$

The values of these decay rates derived from Eq. (15) are

$$\Gamma_d = k_- \tag{27}$$

and

$$\Gamma_m = 2k_+X. \tag{28}$$

To arrive Eq. (28), we have treated the nonlinear term in Eq. (15) in an approximate way, by assuming that the decaying population of initial monomers, $C_m(t)$, interacts with a constant background population of monomers described by the monomer fraction X. We have fit our calculated dimer and monomer correlation functions with the solutions of Eq. (26). The extracted dimer and monomer decay rates are shown in Figures 9 and 10, respectively. At $T^* = 1.5$, there are an insufficient number of bonds in the system to accurately calculate the dimer decay rate, and at $T^* = 0.5$, the dimer decay rate is too slow to get meaningful information from the fit within the time window studied. The extracted dimer decay rate closely follows the reverse rate constant k_- presented in Figure 8. In Figure 10, we have plotted $\Gamma_m/2X$, which should be equivalent to the forward rate constant k_+. Qualitatively, this is found to be the case, although the values in Fig. 10 appear to be systematically faster than those in Fig. 8, especially at lower volume fractions. This discrepancy is likely due to the approximate manner in which the nonlinearity in Eq. (15) was treated in Eq. (28). As noted earlier, the ratio k_+/k_- agrees with Eq. (14) by definition, and therefore the Wertheim prediction. Consequently, the observed deviations between $\Gamma_m/2X$ and k_+ imply that $\Gamma_m/2X\Gamma_d$ exhibits deviations from the Wertheim prediction. We note that, Li and Nies[22] have previously studied the average bonding and unbonding times as a function of association strength for their dimerizing model and that Liu *et al.*[19,20] have studied the temperature and density dependence of the bond lifetime for various association-site models.

As discussed in Subsection VI D, the dissociation of dimers is expected to be an activated process. In order to extract the energy barrier for dissociation, we have fit the temperature dependence of bond lifetime with an Arrhenius function,

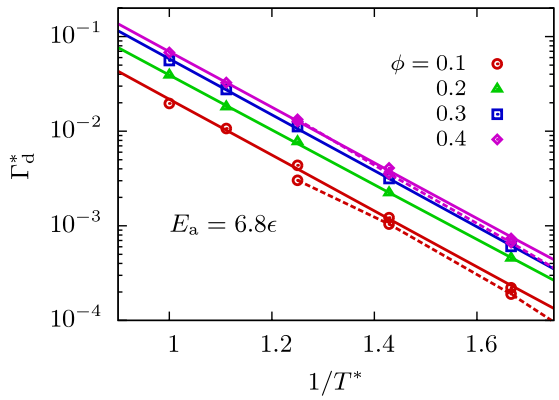

FIG. 9. Arrhenius plot of the reduced dimer decay rate $\Gamma_d^* = \Gamma_d\tau$. The lines are fits to Eq. (29). Dimers decay more quickly at higher volume fractions. These decay rates agree well with the reverse rate constants (dashed lines) plotted in Figure 8.

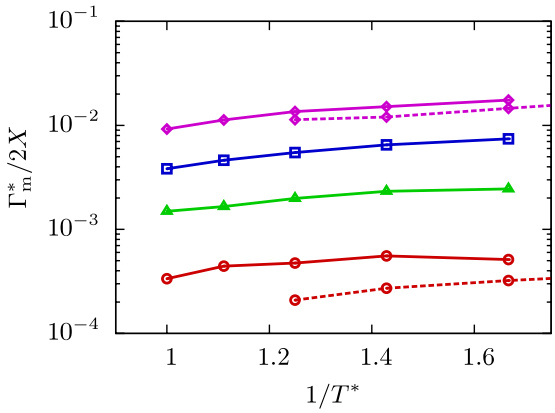

FIG. 10. Arrhenius plot of the scaled monomer decay rate $\Gamma_m^* = \Gamma_m\tau$. The connecting lines are guides to the eye. The meaning of the symbols is the same as in Figure 9. Forward decay rates from Figure 8 are plotted as dashed lines for comparison.

$$\Gamma_d \propto \exp\left(-\frac{E_a}{k_BT}\right), \tag{29}$$

where E_a is the energy barrier to dissociation. These fits are shown in Fig. 9. The average effective depth of the association potential is $E_a = 6.8\epsilon$. This value deviates from the actual potential depth of $A = 10\epsilon$ due to the softened shape of the association potential. The difference between E_a and A is discussed in Subsection VI D.

D. Theoretical considerations regarding $k_\pm$

Here, we attempt to account for the observed volume fraction and temperature dependences of k_+ and k_-. Even though our trajectories are propagated with Hamiltonian dynamics, at the volume fractions studied, the interparticle interactions create an effective drag and a "random" force in the system that can be modeled, at least qualitatively, by Langevin dynamics. From this perspective, the effective drag coefficient γ will increase with increasing ϕ. In order to simplify our discussion of the rate constants, we consider the strong damping limit of the Langevin equation, in which the inverse Langevin drag coefficient, $1/\gamma$, is the shortest characteristic time scale of the system, even though this condition may not rigorously apply to our system. Notably, all of the following arguments hold in the weak damping (Newtonian) limit as well, with changes to coefficients but not the qualitative ϕ and T dependences.

For particles to form bonds, two association sites have to find each other via diffusive processes. If we define an average effective distance between association sites ℓ, the behavior of the forward rate of reaction scales like

$$k_+ \sim \frac{D_s}{\ell^2}. \tag{30}$$

For a dense Langevin system, the volume fraction dependence of the self-diffusion coefficient is given by[33]

$$D_s \simeq \frac{1}{g_0(\sigma)}\left(\frac{k_BT}{m\gamma}\right), \tag{31}$$

where $g_0(\sigma)$ is the radial distribution function of the core reference system evaluated at contact. As an example, the

hard-sphere radial distribution function at contact[34] is well represented by $g_{\mathrm{HS}}(\sigma) \simeq \left(1-\frac{1}{2}\phi\right)/(1-\phi)^3$. We note that $g_0(\sigma)$, like $g_{\mathrm{HS}}(\sigma)$, increases monotonically with ϕ. In this picture, both D_s and ℓ should decrease with increasing ϕ. The fact that k_+ increases with increasing ϕ indicates that ℓ^2 depends more strongly on ϕ than D_s.

An estimate of the reverse rate constant can be framed in terms of Kramers' escape problem.[35] In the strong damping limit, the average escape rate (reverse rate constant) behaves as

$$k_- \sim \frac{\omega_{\min}\omega_b}{\gamma}\exp\left(-\frac{E_a}{k_BT}\right), \tag{32}$$

where $\omega_{\min} = \sqrt{V''_{aa}(r_{\min})/m}$ and $\omega_b = \sqrt{V''_{aa}(r_b)/m}$. For $V_{aa}(r)$ given by Eq. (2),

$$\omega_{\min}\omega_b \sim \frac{A}{md^2}. \tag{33}$$

For the canonical Kramers' problem, the height of the energy barrier is given by $E_a = V_{aa}(r_b) - V_{aa}(r_{\min}) \simeq A$. However, as we will see shortly, interparticle interactions and the shape of the association potential reduce the effective barrier height relative to A. The exponential dependence of the reverse rate on E_a/k_BT is the hallmark of an activated process.

The form of Eq. (4) suggests that the low-temperature ($k_BT \ll A$) equilibrium constant generally behaves as

$$\rho\Delta \sim g_0(\sigma)\exp\left(\frac{E_a}{k_BT}\right). \tag{34}$$

We have fit the values of $\rho\Delta$ obtained from our simulations with Eq. (34) and find $E_a = 6.6\epsilon$. It can be shown that this value of E_a also agrees with Wertheim theory, since $\rho\Delta$ is derivable from the monomer fraction X (cf. Eq. (14) and Fig. 3). The reason E_a differs from the well-depth A stems from the integration in Eq. (4). For short-ranged square-well association sites, the exponential factor, $\exp(A/k_BT)$, can be factored out of the integral in Eq. (4) as an excellent approximation.[15] In contrast, for our soft association sites, this factorization constitutes a poor approximation. The necessary averaging of the Mayer function effectively reduces the barrier height relative to A. These same arguments also account for the comparable activation energy of the dimer decay rate Γ_d.

It is notable that even though the choice of system dynamics, e.g., Newtonian versus Brownian, affects the rate constants k_+ and k_-, the equilibrium constant, $\rho\Delta/2$, is necessarily independent of the choice of dynamics, i.e., the viscosity of the solvent (if any) and the particle mass m do not affect $\rho\Delta/2$. The dependence of k_+ and k_- on the dynamics must therefore cancel out when the ratio is taken in Eq. (14). Based on our scaling estimates, the ratio of rate constants behaves as

$$\frac{k_+}{k_-} \sim \frac{1}{g_0(\sigma)}\left(\frac{d}{\ell}\right)^2\exp\left(\frac{E_a}{k_BT}\right). \tag{35}$$

We note that we have omitted an additional factor of k_BT/A in Eq. (35) since it constitutes a weak temperature dependence in the context of our scaling arguments. The above expression compares favorably with the general behavior of the equilibrium constant, Eq. (34), in several regards. First, it captures the exponential dependence on E_a/k_BT. Second, the manifestly dynamic quantities m and γ cancel out. The volume fraction dependence of Eq. (34) suggests that the effective distance between association sites scales as $\ell \sim 1/g_0(\sigma)$.

We now summarize the implications of our qualitative arguments regarding the behavior of the rate constants. The forward rate constant k_+ increases strongly with increasing ϕ because the effective distance between association sites ℓ decreases with increasing ϕ. Furthermore, k_+ is weakly temperature dependent because the diffusive processes that lead to bond formation are weakly temperature dependent. We note, however, that k_+ actually decreases with increasing T. This behavior is beyond the scope of our simple arguments and clearly indicates the presence of an additional source of temperature dependences, e.g., γ. The strong T dependence of k_- is related to the activated nature of dissociation. The weak ϕ dependence of k_- indicates that dissociation depends more strongly on the internal dynamics of the dimers than on interactions with surrounding particles. The equilibrium constant is characterized by a strong dependence on both ϕ and T. The above results indicate that the strong ϕ dependence can be ascribed to the k_+ contribution and the strong T dependence to the k_- contribution.

VII. CONCLUSIONS AND DISCUSSION

We have investigated and characterized the structure and dynamics of a model dimerizing fluid. A dimer is the simplest type of cluster and is therefore appealing as a reference system for investigations into the dynamics of more complex cluster forming systems. Both the self and the collective relaxation rates are well described by interpolation formulas based on the monomer fraction and the dynamics of permanent monomers and permanent dimers. This indicates that in the region of parameter space explored in this study, the dynamic nature of the bonds does not manifest itself in the relaxation rates (diffusion coefficients). We have also investigated the association kinetics. The forward and reverse rate constants were calculated from non-equilibrium simulations, while the corresponding dimer and monomer lifetimes were calculated from equilibrium simulations. We have also provided a qualitative explanation for the observed temperature and volume fraction dependences of the rate constants.

Yearly *et al.*[10] associated an order of magnitude increase in the viscosity with the formation of dimers in their solutions of monoclonal antibodies. The changes to the self-diffusion coefficient and collective decay rate brought about by dimerization are relatively modest in our system. The pure dimer and pure monomer systems serve as limiting cases for our model. Hence, the properties of the dimerizing system at an arbitrary state point cannot be expected to fall outside of the bounds set by these cases. Only if a dramatic difference between the properties of the monomer and dimer systems exists will a dramatic change be manifested through increased dimerization. For example, the critical volume fraction for an

idealized glass transition is greater for pure monomers than it is for pure dimers.[36] The FISF decay rate goes to zero for both systems as the critical volume fraction is approached. In theory, the relaxation time of a dimerizing system with a volume fraction intermediate to these two critical volume fractions would diverge when the system is forced into a fully dimer state by lowering the temperature.

Apart from the smooth interpolation between the dimer and monomer limits of the diffusion coefficients, we have not observed any signature of the dynamic nature of the bonds, i.e., any dependence on k_+ and k_-. Interestingly, hydrodynamic modifications of the mass balance relation, Eq. (15), predict that the rate constants will affect $\Gamma(Q)$, the collective relaxation rate.[30] However, this result only applies to the fast reaction regime where $k \gg DQ^2$. For the state points and Q values studied, our simulations are solidly in the slow reaction regime. This implies that over the time scale associated with collective diffusion, the dimerization state of the systems is roughly constant, and the system can effectively be treated as a mixture of permanent dimers and permanent monomers.

It is difficult to imagine a scheme by which our simulations can be pushed into the fast reaction regime without employing larger system sizes, which afford access to smaller Q values. Observation of a coupling between diffusion and the rate constants requires a significant number of dimers be present, i.e., $k_+ \simeq k_-$, and that the kinetics are faster than the diffusion rate, $D_s Q^2 < k_\pm$. Combining these requirements with Eq. (30), we find that they are roughly equivalent to $\ell Q < 1$. The product ℓQ can be made small by either moving to smaller Q or by increasing the volume fraction and making ℓ smaller. Even in the fast reaction limit, the small magnitude of the monomer fraction fluctuations, as seen in Fig. 4, would likely impede observation. As can be seen from the estimates of the forward and reverse rate constants, Eqs. (30) and (32), faster dynamics, which correspond to smaller γ, favor larger rate constants. Consequently, dynamic signatures of cluster formation may be even more challenging to find in the Brownian dynamics simulations appropriate for colloidal systems.

We finish with a comment on the different routes to calculating rate constants employed in this work. We have calculated forward and reverse rate constants through both non-equilibrium and equilibrium simulations. Typically, the non-equilibrium calculation of dynamic properties is expected to be more computationally efficient than an equilibrium calculation for the following reason. In the non-equilibrium calculation, one follows the time evolution of an average quantity, in our case, the monomer fraction $X(t)$. In contrast, the typical equilibrium approach to calculating transport properties via a Green-Kubo relation requires the calculation of correlations between the fluctuations, e.g., $\langle \delta X(t) \delta X \rangle$. Since these fluctuations scale like the second moment of the probability distribution, they are computationally more expensive to sample than the average, which scales as the first moment. In our equilibrium calculations of k_+ and k_-, we skirted this problem by focusing on particular constrained subsets of particles (dimers or monomers before first passage) that were treated as being out of equilibrium with the rest of the system in the sense that they obey the mass balance equation Eq. (15). This approach works well for the calculation of non-conserved quantities like the monomer fraction, but cannot be applied to conserved quantities like the density.

ACKNOWLEDGMENTS

C.E.B. acknowledges the support of the National Research Council and thanks Dr. Joseph Curtis for time on computers at the NCNR facility. This manuscript was prepared under cooperative Agreement No. 70NANB10H256 from NIST, U.S. Department of Commerce. The statements, findings, conclusions, and recommendations are those of the authors and do not necessarily reflect the view of NIST or the U.S. Department of Commerce.

[1]E. Bianchi, R. Blaak, and C. N. Likos, Phys. Chem. Chem. Phys. **13**, 6397 (2011).
[2]A. Geiger, P. Mausbach, J. Schnitker, R. L. Blumberg, and H. E. Stanley, J. Phys. Colloq. **45**, C7-13 (1984).
[3]A. Galindo, P. J. Whitehead, G. Jackson, and A. N. Burgess, J. Phys. Chem. B **101**, 2082 (1997).
[4]W. G. Lilyestrom, S. Yadav, S. J. Shire, and T. M. Scherer, J. Phys. Chem. B **117**, 6373 (2013).
[5]L. Hong, A. Cacciuto, E. Luijten, and S. Granick, Langmuir **24**, 621 (2008).
[6]A. I. Campbell, V. J. Anderson, J. S. van Duijneveldt, and P. Bartlett, Phys. Rev. Lett. **94**, 208301 (2005).
[7]F. Sciortino, P. Tartaglia, and E. Zaccarelli, J. Phys. Chem. B **109**, 21942 (2005).
[8]J. T. Cundall, J. Chem. Soc., Trans. **59**, 1076 (1891).
[9]Y. Wang, Y. Wang, D. R. Breed, V. N. Manoharan, L. Feng, A. D. Hollingsworth, M. Weck, and D. J. Pine, Nature **491**, 51 (2012).
[10]E. J. Yearly, P. D. Godfrin, T. Perevozchikova, H. Zhang, P. Falus, L. Porcar, M. Nagao, J. E. Curtis, P. Gawande, R. Taing, I. E. Zarraga, N. J. Wagner, and Y. Liu, Biophys. J. **106**, 1763 (2014).
[11]M. S. Wertheim, J. Stat. Phys. **35**, 19 (1984).
[12]M. S. Wertheim, J. Stat. Phys. **35**, 35 (1984).
[13]M. S. Wertheim, J. Stat. Phys. **42**, 459 (1986).
[14]M. S. Wertheim, J. Stat. Phys. **42**, 477 (1986).
[15]W. G. Chapman, K. E. Gubbins, G. Jackson, and M. Radosz, Fluid Phase Equilib. **52**, 31 (1989).
[16]E. A. Muller and K. E. Gubbins, Ind. Eng. Chem. Res. **40**, 2193 (2001).
[17]N. Kern and D. Frenkel, J. Chem. Phys. **118**, 9882 (2003).
[18]L. Porcar, P. Falus, W.-R. Chen, A. Faraone, E. Fratini, K. Hong, P. Baglioni, and Y. Liu, J. Phys. Chem. Lett. **1**, 126 (2010).
[19]J. Liu, T. L. Bowman II, and J. R. Elliott, Jr., Ind. Eng. Chem. Res. **33**, 957 (1994).
[20]J. Liu and J. R. Elliot, Jr., Ind. Eng. Chem. Res. **35**, 2369 (1996).
[21]T. Li and E. Nies, J. Phys. Chem. B **111**, 2274 (2007).
[22]T. Li and E. Nies, J. Phys. Chem. B **111**, 8131 (2007).
[23]M. S. Wertheim, J. Chem. Phys. **85**, 2929 (1986).
[24]J. Russo, P. Tartaglia, and F. Sciortino, J. Chem. Phys. **131**, 014504 (2009).
[25]See supplementary material at http://dx.doi.org/10.1063/1.4906608 for an additional discussion of simulation details, structural properties, and bonding criterion.
[26]B. Hess, C. Kutzner, D. van der Spoel, and E. Lindahl, J. Chem. Theory Comput. **4**, 435 (2008).
[27]J. P. Boon and S. Yip, *Molecular Hydrodynamics* (McGraw-Hill, 1980).
[28]P. G. de Gennes, Physica **25**, 825 (1959).
[29]D. Chandler and L. R. Pratt, J. Chem. Phys. **65**, 2925 (1976).
[30]B. J. Berne and R. Pecora, *Dynamic Light Scattering* (Dover, 2000).
[31]F. Sciortino, C. De Michele, S. Corezzi, J. Russo, E. Zaccarelli, and P. Tartaglia, Soft Matter **5**, 2571 (2009).
[32]P. van Dongen and M. Ernst, J. Stat. Phys. **37**, 301 (1984).
[33]P. N. Pusey, H. N. W. Lekkerkerker, E. G. D. Cohen, and I. M. de Schepper, Physica A **164**, 12 (1990).
[34]J. P. Hansen and I. R. McDonald, *Theory of Simple Liquids*, 3rd ed. (Academic Press, 2005).
[35]N. G. van Kampen, *Stochastic Processes in Physics and Chemistry*, 3rd ed. ed. (North-Holland, 2007).
[36]S.-H. Chong and W. Götze, Phys. Rev. E **65**, 041503 (2002).